Ocean Dynamics (2014) 64:879–893
DOI 10.1007/s10236-014-0729-2

Spatiotemporal analysis of NORA10 data of significant wave height

Erik Vanem

Received: 19 December 2013 / Accepted: 23 April 2014 / Published online: 24 May 2014

Abstract This paper presents a spatiotemporal analysis performed by applying a Bayesian hierarchical model on NORA10 data of significant wave height. The model has previously been applied to corrected ERA-40 data of significant wave height and was generally found to perform well. However, a new set of high-resolution significant wave height data has recently become available, which is believed to be an improvement compared to the C-ERA-40 data, and a similar spatiotemporal analysis is performed on this new data set. NORA10 differs from C-ERA-40 in various ways and in particular the spatial resolution is significantly increased. Hence, one main motivation for the study presented in this paper is to investigate how the model performs on data with very high spatial resolution. In particular, the model contains a separate component for identifying long-term trends in the wave climate, possibly due to climate change. For the C-ERA-40 data, significant increasing trends were detected in the selected area in the North Atlantic Ocean. These trends are not reproduced in the NORA10 data, but there are differences in geographical and temporal coverage that may, at least partly, explain such differences. The new analysis and the results pertaining to the NORA10 data are presented in this paper.

Responsible Editor: Oyvind Breivik

This article is part of the Topical Collection on the *13th International Workshop on Wave Hindcasting and Forecasting in Banff, Alberta, Canada October 27 – November 1, 2013*

E. Vanem (✉)
DNV-GL, Strategic Research & Innovation,
Veritasveien 1, 1322 Høvik, Norway
e-mail: Erik.Vanem@dnvgl.com

Keywords Ocean waves · Wave statistics · Climate change · Space-time modelling · Long-term trends in the wave climate · NORA10 · Data resolution

1 Introduction

The models presented in this paper are spatiotemporal stochastic models which aim at describing the distribution of significant wave height in space and time. They are fitted to data for an area in the North Atlantic Ocean and estimate the complex spatiotemporal dependence structure at various scales inherent in the data. The models have previously been fitted to corrected ERA-40 data for the North Atlantic (Caires and Swail 2004; Sterl and Caires 2005; Caires and Sterl 2005).

In recent years, it has become increasingly evident that the globe is experiencing a change in climate, mostly due to human activities and emission of greenhouse gases. In this context, it becomes important to understand how such changes may impact the ocean wave climate and subsequently how this may impact the environmental loads on marine structures (Bitner-Gregersen et al. 2012; DNV 2010, 2011; Vanem and Bitner-Gregersen 2012). Hence, the models presented in this report include a component for describing long-term trends in the data for significant wave height. Such trends may then be extrapolated to give indications of possible future trends in the wave climate. Previously, model alternatives with linear and quadratic trend functions (Vanem et al. 2012a), with a log-transform of the data (Vanem et al. 2012b) and with regression on atmospheric CO_2 levels (Vanem et al. 2014) have been

developed and applied to the C-ERA-40 data of significant wave height. The various model alternatives all identified increasing trends in the significant wave height data over the area in the North Atlantic, a finding that has also been substantiated by various time-series trend analyses techniques as presented in (Vanem and Walker 2012). The same modelling framework has also been applied to wind speed data over the same area, as reported in Vanem and Breivik (2013), but failed to identify any significant trends for the windiness. Presumably, this may indicate that the observed increase in waviness is due to increased swell.

In this paper, the Bayesian hierarchical space-time model will be applied to NORA10 data (Reistad et al. 2011, 2007) of significant wave height for an overlapping area of the North Atlantic. The NORA10 is a regional hindcast obtained by dynamical downscaling of the ERA-40 data, producing 3-hourly wave fields at 10–11-km grid spacing. The atmospheric forcing is obtained with the 10-km resolution HIRLAM10 model (Undèn et al. 2002). Compared to the C-ERA-40 data, with a spatial resolution of 1.5 x 1.5° (corresponding to about 167-km grid spacing in lateral direction and between 76- and 105-km grid spacing in longitudinal direction (Vanem et al. 2011)), the NORA10 data has a much higher spatial resolution and is believed to be more accurate. This is supported by (Cavaleri and Bertotti 2003) which generally found that higher data resolution improves the data quality. It has also been reported that the NORA10 data yields significantly higher return values compared to the ERA-40 data (Breivik et al. 2013). One hundred-year return value estimates for the NORA10 data of significant wave height were presented in Aarnes et al. (2012).

By applying the same model on the NORA10 data that has previously been applied to C-ERA-40 data, the results may be compared and the effect of the increased spatial resolution can be evaluated. However, it is emphasized that the difference in resolution is not the only difference between the two data sets and direct comparison might not be reasonable. Of particular interest will be to investigate whether there are long-term temporal trends present in the NORA10 data and to provide estimates of these trends.

2 Data and area description

The study presented in this paper has analysed the NORA10 significant wave height data for a selected area in the North Atlantic Ocean. In the following, the selected area and the data for significant wave height will be described. The models have used regression on CO_2 levels in the atmosphere in order to estimate long-term trends, and both historical CO_2 data and future projections are needed, for fitting the model and for making projections of the wave climate, respectively.

2.1 NORA10 data for significant wave height

The NORA10 data stem from a combined high-resolution atmospheric downscaling and wave hindcast based on the ERA-40 reanalysis over the north-east Atlantic (Reistad et al. 2011). Atmospheric forcing is obtained from the 10-km high-resolution limited area model (HIRLAM10) (Undèn et al. 2002; Furevik et al. 2012) and wave simulations are made by a modified version of the WAM cycle 4 model (Komen et al. 1994), run on the same grid as HIRLAM10 (WAM10). This is nested inside a WAM model at 50-km resolution (WAM50) forced by ERA-40 wind fields covering most of the North Atlantic to account for swell intrusion from the North Atlantic. South Atlantic swell intrusion is neglected.

The NORA10 data set for significant wave height contains 3-hourly wave fields with a spatial resolution of 10–11 km and covers an area in the north-east Atlantic including the North Sea, the Norwegian Sea and the Barents Sea. The complete NORA10 domain is illustrated in Fig. 1, which also indicates the area selected for study in this work (see area description below).

Initially, NORA10 covered the time period September 1957–August 2002, but the NORA10 data set is continually being extended using operational analyses from the European Centre for Medium-Range Weather Forecasts (ECMWF) as boundary and initial conditions (Aarnes et al. 2012). Hence, the NORA10 data set analysed in this paper spans the period January 1958–December 2012, and the actual analysis considers data from January 1959 to December 2012. Data for the year 1958 were excluded from the analysis because CO_2 data were not available before March 1958. For the purpose of fitting the Bayesian hierarchical model, monthly maximum data have been used, and the monthly maxima at each spatial location have been extracted for each month of the 55-year period 1958–2012. Hence, time-series of 660 data points in time for each of the 2,601 spatial grid points, totalling 1,716,660 data points in space and time, extracted from NORA10 form the basis for the analysis presented herein. However, due to time-consuming simulations, the spatial resolution has been reduced before running the simulations, as outlined below.

Comparison with in situ measurements and satellite observations is reported in Reistad et al. (2011) and reveals that the NORA10 data yield a significant improvement compared to the ERA-40 data. For example, the ERA-40 data consistently underestimate the mean wave height, a bias that is not reproduced by the downscaling. Furthermore, root mean square errors are higher for the ERA-40

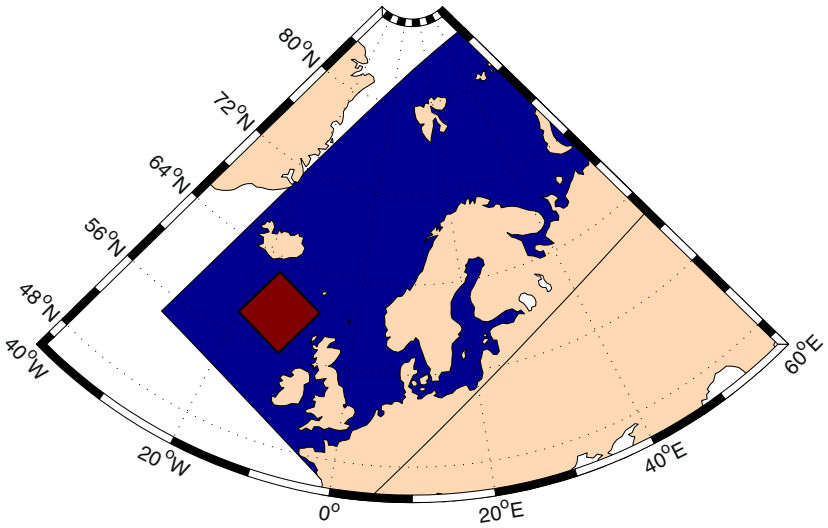

Fig. 1 The NORA10 model domain

data compared to NORA10. Hence, it is assumed that the NORA10 represents a significant improvement compared to ERA-40 and that the NORA10 data are superior. In particular, it is well accepted that the upper percentiles of the significant wave height distribution are underestimated by ERA-40 and NORA10 yields significantly higher return values. Comparison of significant wave height from ERA-40 and the coarser WAM50 indicates a very close correlation

2.1.1 Comparison with C-ERA-40 data

NORA10 was forced on the boundaries with ERA-40 data, and therefore, the NORA10 data for significant wave height should in some sense be consistent with the ERA-40 data. Hence, it would in principle make sense to compare the outcome of statistical analyses of the two data sets. However, the C-ERA-40 data set was obtained by adjusting the ERA-40 data to buoy and altimeter measurements. In particular, it has been observed that the ERA-40 data underestimate high values and that there exist inhomogeneities in the time series due to the assimilation of different altimeter data sets (Caires and Sterl 2005). Both these features have been improved in the C-ERA-40 data. Earlier efforts on correcting reanalysis data sets have focused on improving the wind fields and then use the corrected wind fields to force wave models (Swail and Cox 2000; Wang and Swail 2002). It has been reported that such efforts yield improved comparison with observations (Caires et al. 2004), but at a considerable cost. The C-ERA-40 data, on the other hand, were obtained by correcting the ERA-40 significant wave height fields directly, based on assumptions of conditional stationarity and a training data set consisting of both ERA-40 data and measurements (and hence also estimated errors). Even though these corrections are reported to improve the ERA-40 data considerably, it also means that the C-ERA-40 data are not consistent with the ERA-40 data and hence neither with the NORA10 data obtained by forcing ERA-40 on the boundaries.

Another major difference between the NORA10 data and the C-ERA-40 data is the data resolution. Both the spatial and the temporal resolution of the NORA10 data are considerably higher than for the C-ERA-40 data. The orientation of the data grid is also different. C-ERA-40 data lie on a cylindrical grid with grid points 1.5° apart, whereas the NORA10 data lie on a rotated spherical equidistant grid, with a spatial separation of 10 km. Furthermore, the NORA10 data cover a different time span and in particular include 10 years of more recent data compared to the C-ERA-40 data. Finally, as will be outlined in the subsequent subsection, the geographical coverage of the analyses on the C-ERA-40 data and the NORA10 data are different, although partly overlapping.

All these differences make direct comparison of the results for the two data sets difficult; there is a priori no reason to expect similar results from the statistical models for the two data sets. Nevertheless, the previous results obtained from an analysis of the C-ERA-40 data will be referred to in this paper, and in some sense compared to the NORA10 analysis. It is emphasized that the purpose of this comparison is not to validate or verify either of the results, or the statistical models, in any way, but the differences in results are believed to be of interest in itself.

2.1.2 North-Atlantic area selected for the analysis

The area selected for this analysis is an area in the North Atlantic Ocean that is partly overlapping with the area that

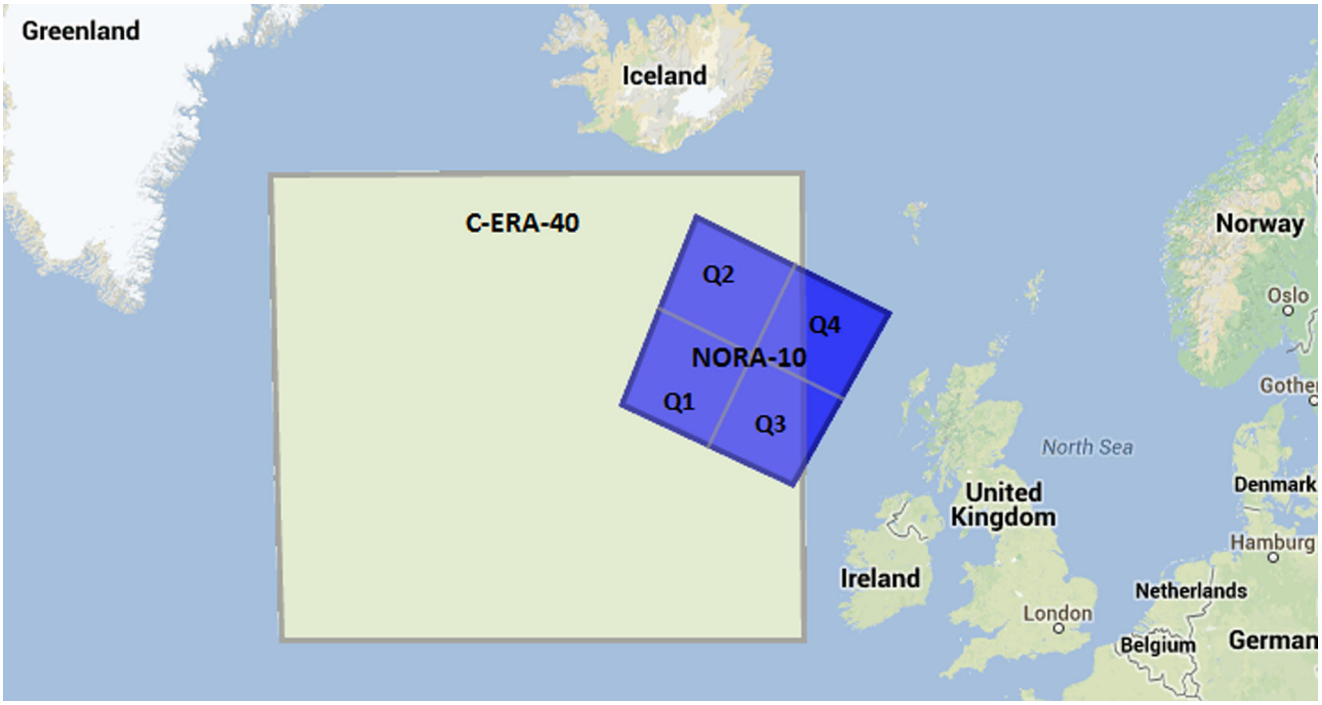

Fig. 2 Areas in the North Atlantic selected for study. The area analysed with C-ERA-40 data (*green*) and the area analysed with NORA10 data (*blue*)

was selected for analysis with the C-ERA-40 data. It has been chosen so that the area is some distance away from the boundary of the NORA10 model domain so that possible edge-effects are minimized. The area analysed by the NORA10 data is shown in Fig. 2, where also the area that has previously been investigated based on C-ERA-40 data is included for reference.

As can be seen from Fig. 2, the geographical area considered for the NORA10 data is much smaller than the area for the C-ERA-40 data. However, due to the much higher resolution of the NORA10 data, this area contains a much larger number of grid points. The blue area in the figure contains 51 x 51 = 2601 NORA10 data points whereas the larger green area contains 9 x 17 = 153 C-ERA-40 data points. Thus, the analysed NORA10 data contain 17 times more spatial data-points than the C-ERA-40 data.

The NORA10 data lie on a rotated spherical equidistant grid, with a spatial separation of 10 km between grid points in both directions. This means that the grid points do not correspond to integer longitude and latitude, but the geographical distance between neighbouring points is constant throughout the grid. The coordinates of the four corners of the NORA10 area are given in Table 1. The C-ERA-40 data, on the other hand, lie on a cylindrical grid, between 51 and 63° north and 12 and 36° west, with about 167-km grid spacing in lateral direction and between 76 (northernmost) and 105 (southernmost) km grid spacing in longitudinal direction (Vanem et al. 2011).

Even though the area for the NORA10 data is much smaller than the area previously analysed with C-ERA-40 data, the much higher resolution means that the amount

Table 1 Coordinates of the corners of the NORA10 area; (degrees North, degrees East)

Corner	West	East
North	(62.59, 16.37)	(60.39, 6.97)
South	(57.9, 19.87)	(55.99, 11.5)

Table 2 Coordinates of the edges of the quarter-areas; (°N, °E)

Quarter-area	Coordinates of the edges	
Q1	(60.17, 18.34)	(59.26, 13.93)
	(57.90, 19.87)	(57.06, 15.74)
Q2	**(62.59, 16.37)**	(61.62, 11.69)
	(60.35, 18.18)	(59.45, 13.77)
Q3	(59.18, 13.58)	(58.12, 9.47)
	(56.99, 15.40)	**(55.99, 11.50)**
Q4	(61.53, 11.32)	**(60.39, 6.97)**
	(59.36, 13.41)	(58.30, 9.29)

Bold numbers correspond to the corners of the overall area (Table 1)

Table 3 Average monthly maxima for individual months in the NORA10 data and comparison with C-ERA-40 data. Minimum and maximum monthly maximum significant wave height for individual months (m)

	Jan	Feb	Mar	Apr	May	Jun	Jul	Aug	Sep	Oct	Nov	Dec	Overall
NORA10	10.6	10.0	9.09	7.30	6.23	5.27	4.95	5.33	7.60	8.75	9.40	10.2	7.89
C-ERA-40	9.87	8.91	7.18	5.89	5.89	5.03	4.42	5.04	6.96	8.21	8.69	9.79	7.48
Difference	0.73	1.09	1.91	1.41	0.34	0.24	0.53	0.29	0.64	0.54	0.71	0.41	0.41
Min	5.9	5.0	4.5	4.1	3.0	2.6	2.4	2.6	4.0	3.6	5.0	5.6	2.4
Max	21.7	17.4	16.3	13.0	13.0	10.0	10.2	11.5	14.5	15.0	18.7	18.5	21.7

of spatial data is significantly higher. This slows down the computation and it was decided to run five sets of simulations. First, the NORA10 area is divided into four quarters and simulations are run separately for each quarter-area with half the spatial resolution, corresponding to four areas with 13 x 13 = 169 grid points. Subsequently, simulations are run on the whole area with reduced spatial resolution, i.e. using every fourth data-point to obtain a grid with 40-km separation between the grid points. The results for the complete area can then be compared with the results pertaining to each of the quarter-areas. The coordinates of the corners in each of the quarter-areas are given in Table 2, and the quarter-areas are indicated in Fig. 2.

2.1.3 Initial data analysis

A brief initial data inspection reveals that the mean significant wave height in the data set described above is 7.9 m (monthly maximum data). This is higher than for the C-ERA-40 data where the mean value was 7.5 m. The minimum value is 2.4 m and the maximum value is 21.7 m in the NORA10 data.

The average monthly maxima for individual months in the NORA10 data are given in Table 3. Included in the table are also the corresponding averages for the C-ERA-40 data for comparison (Vanem 2013), and it is interesting to observe that the monthly maxima from the NORA10 data are consistently higher than for the C-ERA-40 data; for each individual month, the average monthly maximum over the data period is higher in the NORA10 data. Differences range from 0.24 m to as much as 1.91 m for the month of March. Overall, the average monthly maximum is 41 cm higher in the NORA10 data. The minimum and maximum values for individual months (monthly maximum for the NORA10 data) are also presented in Table 3.

The density of the monthly maximum data from NORA10 is shown in Fig. 3, where also the density for the monthly maximum data from C-ERA-40 is included for reference. It is seen that the densities are largely overlapping even though the NORA10 density seems to be slightly shifted towards higher values. This confirms that the NORA10 data generally have slightly higher values for the monthly maximum significant wave height.

Identifying and estimating possible long-term trends in the data are of particular interest. Figure 4 illustrates a crude approach where straight lines are fitted by least squares to time-series of spatial mean, spatial maxima and spatial minima of the NORA10 data. The estimated intercepts and slopes of the fitted lines as well as the associated accumulated trends over the data period are presented in Table 4. This crude exercise suggests that there are increasing trends in the spatial min, mean and max time series, with highest trends for the spatial maxima at almost 70 cm over the data period. For the average, an estimated overall trend of about 29 cm is obtained in this way. However, the time series are quite noisy, and the p values of the estimated trends

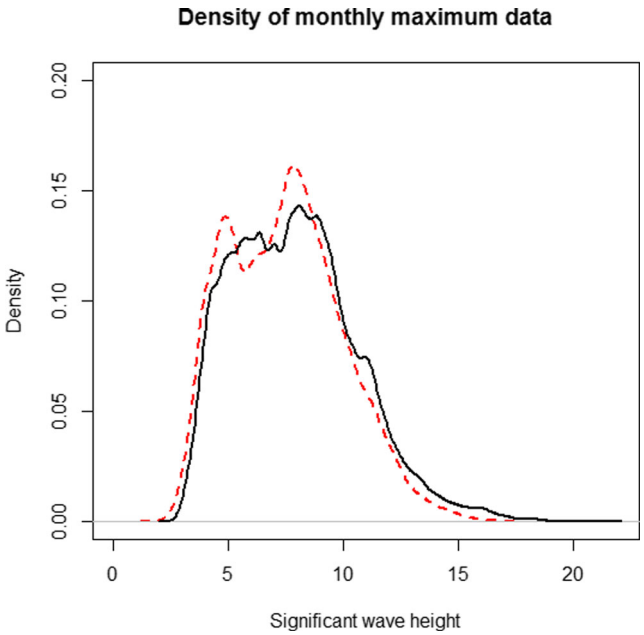

Fig. 3 The density of the NORA10 data for monthly maximum significant wave height (*black line*). For comparison, the density of the C-ERA-40 data is also shown (*red dotted line*)

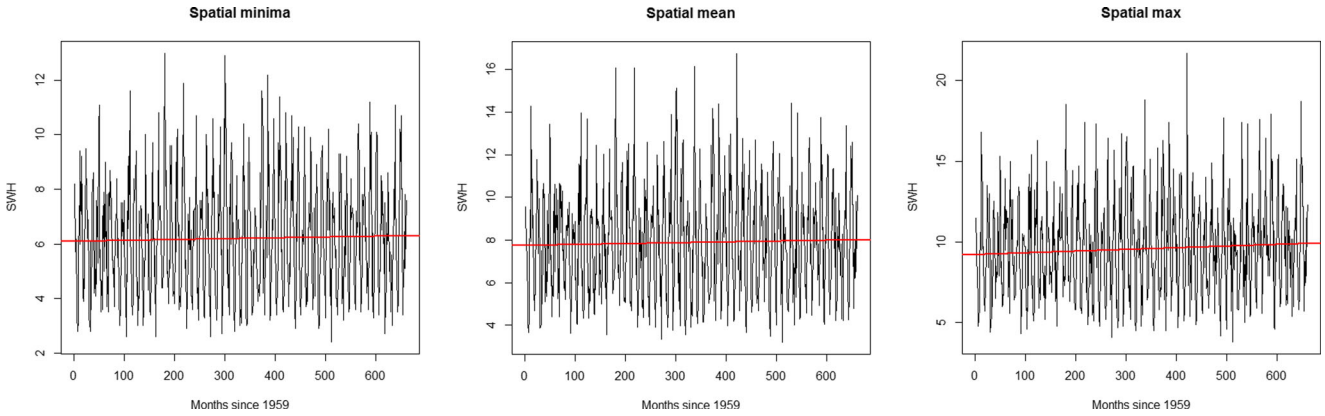

Fig. 4 Initial trend analysis: Fitting a straight line by least squares to time series of spatial minima (*left*), spatial averages (*middle*) and spatial maxima (*right*)

are 0.398 (spatial min), 0.463 (spatial mean) and 0.0854 (spatial max), respectively. Hence, even though the least square approach estimates an increasing trend in the data, the trends are not found to be statistically significant at 95 or 99 % significance level. For the spatial maxima, the trend is statistically significant at the 90 % level, but the spatial minima and mean fail to be significant at any reasonable significance level.

It is noted that when straight trend-lines were fitted by least squares for the C-ERA-40 data, the estimated trends were found to be statistically significant at 99 % level (p values were not reported in Vanem and Walker (2012), but all were very small).

2.2 CO_2 data

Concentrations of atmospheric CO_2 have been used as covariates for explaining possible long-term trends in the significant wave height data, and basically two sets of data have been exploited: historic data for model fitting and projections of future concentration levels for future predictions. The same CO_2 data were used in the analysis of the C-ERA-40 data, as described in Vanem et al. (2014).

Table 4 Estimated parameters of straight lines fitted by least squares and corresponding trends

	Spatial min	Spatial mean	Spatial max
Intercept	6.1058	7.7474	9.2130
Slope	0.0003138	0.0004393	0.001056
p value of the slope	0.398	0.463	0.0854
Annual trend (cm)	0.3765	0.5272	1.268
Accumulated trend (cm)	20.71	28.99	69.72

2.2.1 Historic data

For the purpose of this study, monthly average CO_2 data from the Mauna Loa Observatory, Hawaii, which has the longest continuous record of direct atmospheric CO_2 measurements, have been used (Thoning et al. 1989). Data are available from March 1958 to present, on the format of parts per million (ppm), and monthly trend time series will be used. The seasonal cycle in the monthly maximum significant wave height is accounted for in a separate seasonal component in the Bayesian hierarchical model. The monthly trend CO_2 time series are shown in Fig. 5. It is noted that the CO_2 data for 1958 are not complete and therefore the analysis reported herein will start from January 1959.

It is noted that the data stem from observations outside of the area in the North Atlantic which is the focus of this study. However, it is assumed that CO_2 is well mixed in the atmosphere, and that this does not introduce any notable bias in the monthly trend values or influence the results of the analysis.

2.2.2 Future projections

In order to make projections of future wave climate, future projections of the covariates are needed and projections of the atmospheric concentration of CO_2 will be exploited. Future predictions are of course uncertain and different projections of CO_2 levels have been made based on different emission scenarios. For the purpose of this study, projected emissions and concentrations presented by IPCC for the four marker scenarios (A1B, A2, B1 and B2), obtained from the ISAM carbon cycle (Jain et al. 1995), have been considered. It is observed that the scenarios A2 and B1 correspond to the highest and lowest projected CO_2 levels, respectively, and it is therefore assumed sufficient to employ these two in

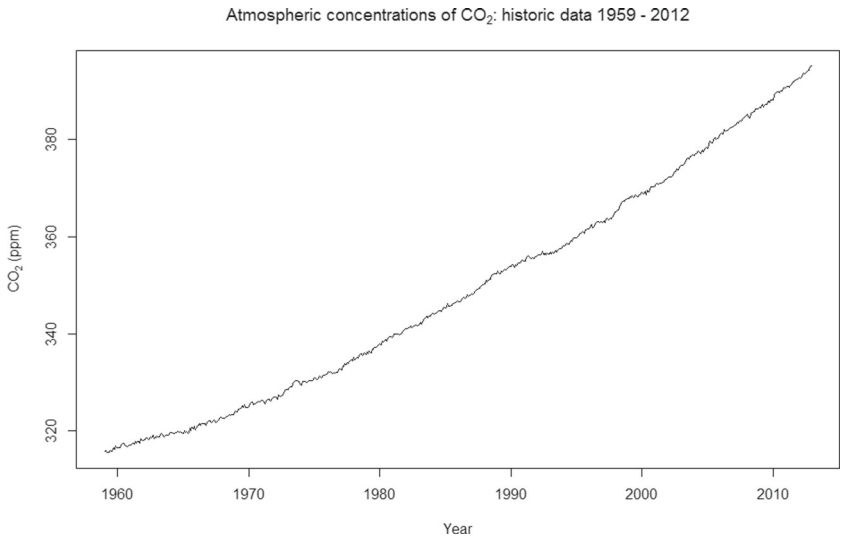

Fig. 5 Historic CO_2 concentrations in the atmosphere, 1959–2012

the modelling, as the other scenarios will fall between these. Scenario A2 might be an extreme scenario, but from a precautionary perspective, it is important to include this in the analysis as this could be construed as a worst case scenario. The CO_2 projections data can also be found in appendix II of the report (IPCC 2001).

The projected levels of atmospheric CO_2 concentrations are given for every 10 year towards 2100. For the purpose of this study, monthly averages are needed, and simple linear interpolation within each decade has been used in order to estimate monthly projections. The decadal projections are then assumed as the value for January of that year. In this way, monthly projections of CO_2 levels in the atmosphere from year 2013 until 2100 are obtained for use as covariates in the regression component of the stochastic model for significant wave height. The interpolated monthly projections are plotted in Fig. 6.

3 The Bayesian hierarchical space-time model

Various versions of the statistical model used in analysing the data have previously been presented in other papers, and will only be briefly presented in the following. The model used in this study is essentially equivalent to the one presented in Vanem et al. (2014), where regression on atmospheric CO_2 levels is included.

The spatiotemporal data are indexed by two indices; an index x to denote spatial location ($x = 1, 2, \ldots, X = 169$ in the simulations reported herein), and an index t to denote a point in time (i.e. months, $t = 1, 2, \ldots, T = 648$ for monthly maxima data in the simulations reported herein). All the stochastic terms introduced in the model are assumed mutually independent and independent in space and time, having a zero-mean Gaussian distribution with some random, but identical variance, i.e. with generic notation $\varepsilon_\beta \overset{i.i.d}{\sim} N(0, \sigma_\beta^2)$. It should be understood that the model is defined $\forall x \geq 1, t \geq 1$, as relevant for each component.

3.1 Model description

At the first level, the observations (monthly maximum significant wave height), Z at location x and time t, are modelled in the observation model as the latent variable H, corresponding to the underlying significant wave height

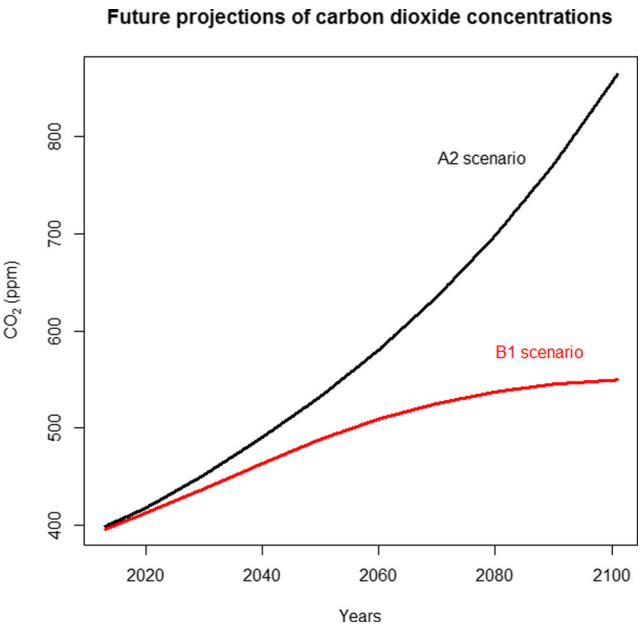

Fig. 6 Future projections of CO_2 concentrations in the atmosphere; A2 and B1 scenarios from 2013–2100

process, and some random noise, ε_Z, which may be construed to include statistical measurement error:

$$Z(x,t) = H(x,t) + \varepsilon_z(x,t) \tag{1}$$

The underlying process for the significant wave height at location x and time t is modelled by the state model, which is split into a time-independent component, $\propto(x)$, a space-time interaction component, $\theta(x,t)$ and spatially independent components $M(t)$ and $T(t)$ for seasonal and long-term trend contributions, respectively, as shown in Eq. 2. The long-term trend component is assumed spatially invariant and can possibly be partly related to the effect of climate change on the ocean wave climate.

$$H(x,t) = \propto(x) + \theta(x,t) + M(t) + T(t) \tag{2}$$

The time-independent spatial field is modelled as a first-order Markov Random Field (MRF), conditional on its nearest neighbours in all cardinal directions, and with different dependence parameters in lateral and longitudinal directions, as shown in Eq. 3. Even though the data is on a rotated grid so that the data points do not strictly lie along north-south and east-west lines, the following notation has been used: x^D = the location of the nearest grid point in direction D from x, where $D \in \{N, S, W, E\}$ and N = 'North', S = 'South', W = 'West' and E = 'East'. Hence, for instance the point x^N should be construed to be the nearest grid point immediately to the north-east of x (see Fig. 2). The other directions are rotated in a similar way from the strictly north-south/east-west coordinate system. If x is at the border of the area, the value at the corresponding neighbouring grid point outside the area is taken to be zero, hence no particular measures are taken to correct for edge effects.

$$\begin{aligned}\propto(x) =& \propto_0(x) + a_\phi \left\{ \propto(x^N) - \propto_0(x^N) + \propto(x^S) - \propto_0(x^S) \right\} \\ &+ a_\lambda \left\{ \propto(x^W) - \propto_0(x^W) + \propto(x^E) - \propto_0(x^E) \right\} + \varepsilon_\propto(x)\end{aligned} \tag{3}$$

a_ϕ and a_λ are spatial dependence parameters in the main directions of the grid, i.e. lateral (northeast–southwest direction as from areas $Q1 \leftrightarrow Q2$ in Fig. 2) and longitudinal (southeast–northwest direction as from areas $Q1 \leftrightarrow Q3$) directions, respectively. The spatially specific mean $\propto_0(x)$ is modelled by a spatial trend function with a quadratic form and an interaction term in the rotated grid. Letting $m(x)$ and $n(x)$ denote the relative ordering within the grid in either direction of location x (with $n(x), m(x) \in \{1, 2, \ldots, 13\}$ for a grid of size $13 \times 13 = 169$), the spatially specific mean is modelled by Eq. 4, where $\propto_{0,i}, i = 1, \ldots, 6$ are parameters to be estimated from the data.

$$\begin{aligned}\propto_0(x) =& \propto_{0,1} + \propto_{0,2} m(x) + \propto_{0,3} n(x) + \propto_{0,4} m(x)^2 \\ &+ \mu_{0,5} n(x)^2 + \mu_{0,6} m(x) n(x)\end{aligned} \tag{4}$$

The spatiotemporal dynamic term $\theta(x,t)$ is modelled as a vector autoregressive model of order one, conditionally specified on its nearest neighbours in all cardinal directions, as shown in Eq. 5; $b.$ are model parameters.

$$\begin{aligned}\theta(x,t) =& b_0\theta(x,t-1) + b_N\theta\left(x^N, t-1\right) \\ &+ b_E\theta\left(x^E, t-1\right) + b_S\theta\left(x^S, t-1\right) \\ &+ b_W\theta\left(x^W, t-1\right) + \varepsilon_\theta(x,t)\end{aligned} \tag{5}$$

The temporal component is modelled with a seasonal and a long-term trend part. The seasonal part is modelled as a combination of an annual and a semi-annual cyclic contribution (i.e. including the first two harmonic components) where the seasonal contribution is assumed invariant in space, as described by Eq. 6. c, d, f and g are model parameters to be estimated from the data and ω corresponds to an angular frequency with period 1 year.

$$\begin{aligned}M(t) =& \; c\cos\omega t + d\sin\omega t + f\cos 2\omega t \\ &+ g\sin 2\omega t + \varepsilon_m(t)\end{aligned} \tag{6}$$

In order to include and isolate possible long-term effects of climate change in the model, a regression component on CO_2 concentrations in the atmosphere has been included, assuming a combination of a linear and logarithmic relationship between the trend and the concentration level (Eq. 7). Different alternatives for this component were investigated in Vanem et al. (2014), e.g. including a quadratic term and purely linear or logarithmic terms, and the linear-log form was found to be superior for the C-ERA-40 data. Hence, only this model alternative has been employed in the current analysis of the NORA10 data. $G(t)$ denotes the average level of CO_2 in the atmosphere at time t (month) and γ and η are model parameters. It is acknowledged that CO_2 is known to mix well in the atmosphere, so there is no spatial component in this regression term.

$$T(t) = \gamma G(t) + \eta \log G(t) + \varepsilon_T(t) \tag{7}$$

3.2 Prior distributions

Prior distributions are assigned in order to account for uncertainties in the model parameters, and all inference and predictions are made on the posterior distribution. Hence, specifying prior distributions on all the model parameters, together with specification of initial values for $\theta(x,0)\ \forall x$, completes the specification of the model. Prior distributions for all model parameters are assumed independent, and conditionally conjugate priors will be specified for most priors to ensure that the conditional posterior distributions will be straightforward to derive. It is noted that the amount of data is quite large in this case and that therefore, the posteriors are not believed to be very sensitive to the exact values of

the hyper-parameters; it is well known in Bayesian statistics that the posteriors are asymptotically independent of the priors as the amount of data increases. Similar priors as in previous studies have been used (Vanem 2012, 2013), and details are not included in this paper.

3.3 Model implementation

Having completed the model specification and specified the priors, the derivation of the full conditionals for each model parameter is quite straightforward, as outlined in the appendix of Vanem (2013). Samples from the posteriors can then be obtained using MCMC methods, i.e. the Gibbs sampler with additional Metropolis-Hastings steps.

The MCMC methods for generating samples from the posterior distribution and hence inferring and making predictions from the model have been implemented in Java. Post-processing of the results, including preparation of plots, has been performed in **R**.

3.4 Simulation setup

As discussed above, five different subsets of the data have been investigated individually in order to reduce the computation time; trying to run the model for the full dataset causes computations to become extremely time consuming and also increases the time for the MCMC chains to converge. Hence, the five subsets of (monthly maximum) data that have been analysed are as follows (see Fig. 2):

- The complete area, but with every fourth data point in space (totalling 13 x 13 = 169 locations)
- Sub-area Q1 with every second data point in space (169 locations)
- Sub-area Q2 with every second data point in space (169 locations)
- Sub-area Q3 with every second data point in space (169 locations)
- Sub-area Q4 with every second data point in space (169 locations)

The MCMC simulations were run with a burn-in period of 40,000 samples and a batch size of 20. Hence, a total of 60,000 iterations were run to obtain a total of 1,000 samples of the posterior parameter vector. In each iteration, the additional Metropolis-Hastings steps that were introduced to sample from the a_ϕ and a_λ parameters were repeated six times. This yields overall acceptance rates between 73 and 79 % for the various simulation runs, which is more than sufficient to obtain good mixing properties of the chains.

Trace plots from the marginal sampled posterior distributions indicate stationarity and it is believed that the burn-in period is sufficient for the chain to converge. In the previous analyses of the C-ERA-40 data, some control runs were performed that indicated that burn-in periods far less than what has been employed in this study resulted in stationary chains and it is therefore assumed that convergence is likely also in the present study. However, the spatial fields are larger and might therefore need longer time to converge. Normal probability plots indicate that the Gaussian model assumption might be realistic.

With the settings above, simulations of the different sub-data sets with dimensions $169 \times 648 = 109{,}512$ data points complete well within a day.

4 Results and predictions

In this section, the results from the simulations of the different sub-sets of data will be presented. First, the results pertaining to the complete area, where every forth location was used will be presented. This can then be compared to the results for each of the four sub-areas that has been analysed with higher spatial resolution.

It is noted that the long-term trend contribution does not necessarily start at 0, so the estimated values of the time-independent contributions, $\propto(x)$, are adjusted to incorporate the mean value of the estimated trend component at year 2012 (see also the discussions in Vanem et al. (2014, 2012c).

4.1 Complete area

The following results are from simulations run over the complete selected area, using every fourth grid-point in space.

The six parameters $\propto_{0,\cdot}$ determine the spatially varying mean $\propto_0(x)$ over the selected area. Together with the spatial dependence parameters a_ϕ and a_λ, they determine the time independent spatial field $\propto(x)$. The estimated mean of this field for the complete selected area is illustrated in Fig. 7, where the x- and y-directions corresponds to the axes of the rotated grid with the NORA10 data. The results indicate that there are relatively small spatial variations over the area, with estimated values of the mean spatial field ranging from 7.5 to 7.8 m over the area, with a mean value of 7.7 m.

For the space-time interaction component, the mean contribution from this term ranges from -2.1 to 1.4 m over all locations and time points (except $t = 0$). The average contribution is close to zero as it should, and the variances range from 0.047 to 0.37 m^2. This seems reasonable and a notable part of the modelled significant wave height can be ascribed to this component.

The estimated contribution from the seasonal component, $M(t)$, is shown in Fig. 8 for the first 10 years, displaying a

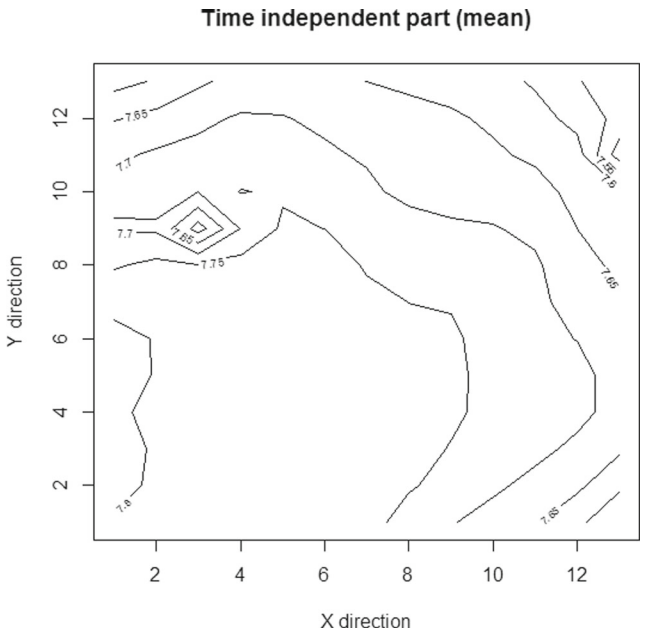

Fig. 7 The estimated spatial random field, $\propto(x)$, for the complete area

clear cyclic behaviour. The estimated seasonal contribution varies between −3.0 and 2.5 m corresponding to a mean annual variation in the range of 5.5 m for the monthly maximum data. The asymmetry between the seasonal minima and maxima is picked up by the model due to the inclusion of the second harmonic in the seasonal component, which is then warranted.

The estimated long-term trend over the period covered by the NORA10 data is illustrated in Fig. 9, including the mean and 90 % credible intervals of the estimated trend. The trend contribution is adjusted so that it starts at zero. It is observed that the estimated trend signal is quite noisy, but that a mean increasing trend can be extracted. The estimated mean long-term trend over the data period is 21 cm, with a 90 % credible interval ranging from −5.6 to 48 cm. Hence, even though the model extracts an increasing trend in the wave climate, this trend is not statistically significant at the 90 % level.

Assuming that the observed stochastic relationship between significant wave height and atmospheric levels of CO_2 remains unchanged in the future, future projections of significant wave height can be made based on different future emission scenarios. Projections obtained in this way by adopting the IPCC A2 and B1 scenarios, respectively, are illustrated in Fig. 10. With both scenarios, the mean future trend is increasing. It is observed that the extreme emission scenario A2 yields a higher expected future trend (note that the scales on the two figures are different), but that neither of the future trends are statistically significant at the 90 % level. For the A2 emission scenario, the estimated mean accumulated trend between 2012 and 2100 corresponds to an increase of 1.4 m, with 90 % credible intervals ranging from a decrease of 1.2 m to an increase of 3.5 m. The corresponding mean future increase estimated by assuming the B1 emission scenario is 43 cm, with 90 % credible intervals ranging from a decrease of 48 cm to an increase of1.2 m.

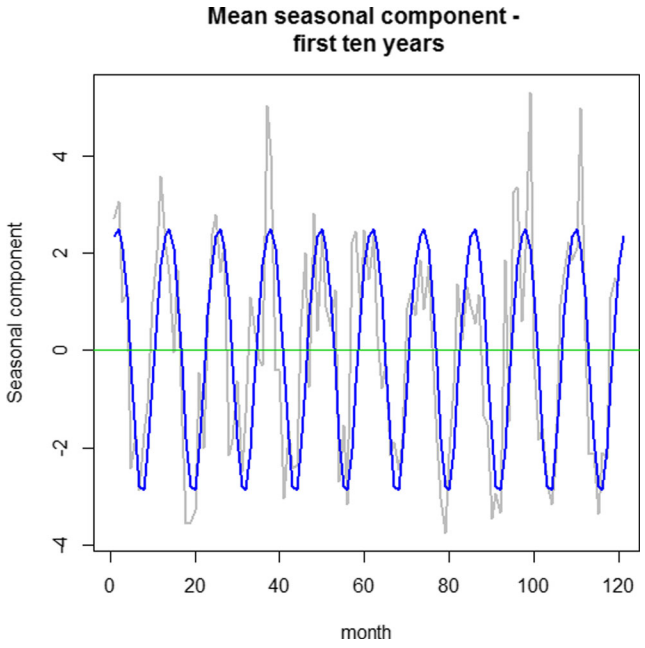

Fig. 8 The estimated seasonal contribution for the first 10 years (complete area)

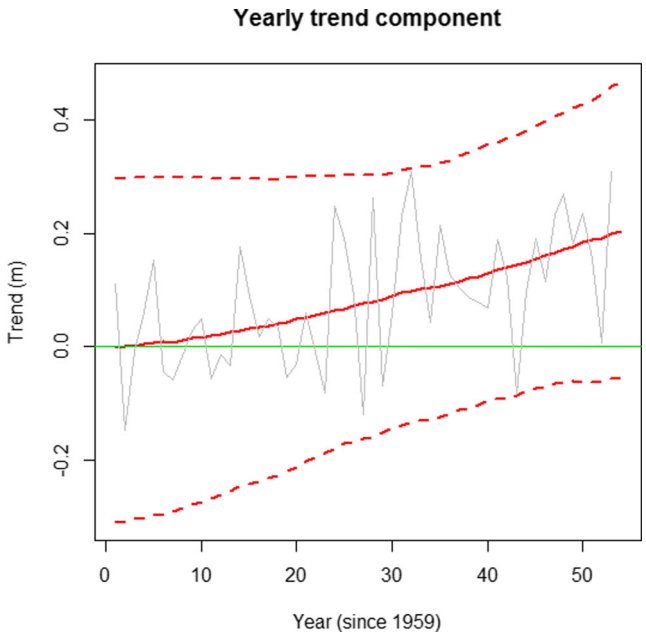

Fig. 9 Estimated long-term trend for the complete selected area

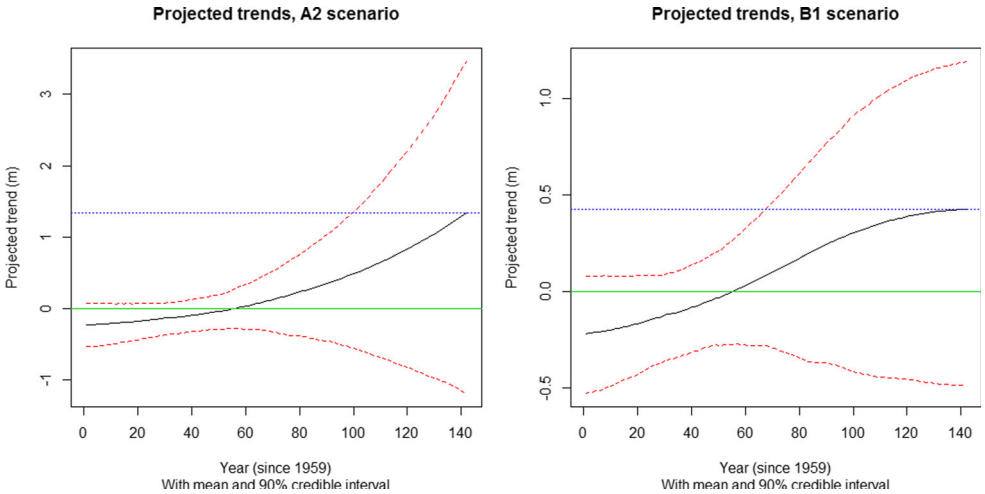

Fig. 10 Projected future trends in the significant wave height for the complete area

4.2 Sub-areas

In addition to running the Bayesian hierarchical space-time model on the complete selected area of NORA10 data, separate simulations have been run on four sub-areas, referred to as Q1 to Q4 (see Fig. 2). The setup of the simulations is identical to the simulations for the whole area and the results will be reported in the following. Since the sub-areas are obviously smaller in extension than the whole area, the spatial resolution has been doubled compared to the simulations for the whole area without increasing the computational time. Hence, the spatial grids are of the same size as before, but with shorter distances between grid points. A brief summary of the results for the various sub-areas is given below.

The estimated mean spatial fields are presented in Fig. 11 for all sub-areas. For the rest of the components, the figures are very similar to the ones for the complete area, and figures will not be presented. The ranges of estimated values for the different model components for each of the sub-areas are also included in Table 5. Also the estimated 90 % credible intervals for the long-term trends (1959–2012) and the future projections (2013–2100) are presented in Table 5.

4.3 Simulations with RCPs as predictors for the long term trend

Another set of simulations has also been performed where total radiative forcings consistent with the recently proposed representative concentration pathways (RCP; (Moss et al. 2010; van Vuuren et al. 2011)) were used as predictors for the long-term trends rather than CO_2 levels from various emission scenarios. However, changing the explanatory variables in this way did not change the overall results that there are no significant trends in the NORA10 data for significant wave height for the analysed area. Hence, the details of these simulations are not presented in this paper and they do not provide any essential new information.

5 Discussion and comparison of results

5.1 Comparison of results for the complete area and the different sub-areas

The simulations presented in the preceding sections use different sub-sets of data, which all stem from the same source,

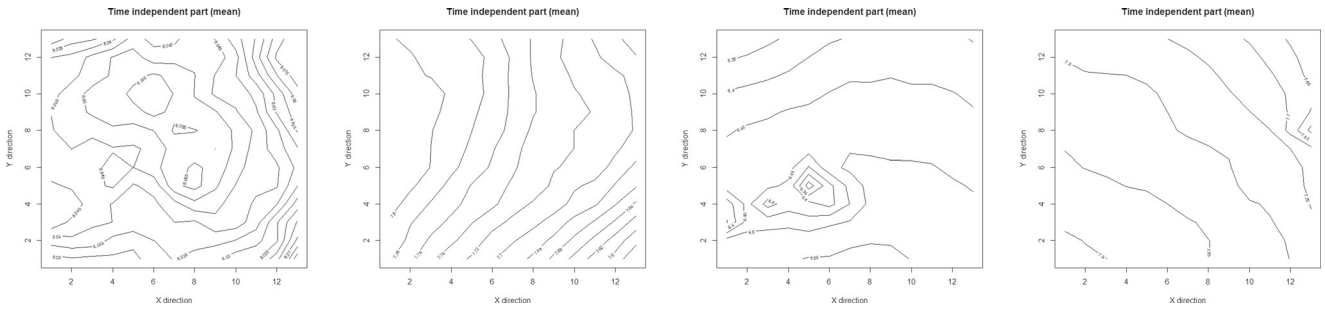

Fig. 11 The estimated mean spatial field for sub-areas Q1 (*left*)–Q4 (*right*)

Table 5 Range of estimated values for the different model components (m)

	Complete area	Q1	Q2	Q3	Q4
Spatial field	7.5–7.8	8.0–8.1	7.6–7.8	6.3–6.6	7.6–7.9
$\theta(x, t > 0)$	−2.1–1.4	−1.1–0.70	−0.72–0.81	−1.6–1.2	−0.95–0.97
Seasonal component	−3.0–2.5	−3.0–2.5	−3.0–2.5	−2.9–2.4	−3.0–2.5
Long-term trend	0.21	0.04	0.16	0.11	0.35
A2 projections	1.4	0.27	1.0	0.61	2.3
B1 projections	0.43	0.09	0.33	0.20	0.72
Trend: 90 % c.i.	−0.056–0.48	−0.23–0.33	−0.14–0.54	−0.14–0.32	0.025–0.62
A2: 90 % c.i.	−1.2–3.5	−2.5–3.2	−1.4–4.1	−2.5–3.2	−0.97–4.7
B1: 90 % c.i.	−0.48–1.2	−0.95–1.1	−0.6–1.6	−0.97–1.2	−0.51–1.7

the NORA10. The differences are in spatial resolution and geographical location, with the four sub-areas essentially constituting the overall area.

The average spatial fields, $\propto(x)$, were estimated to be slightly different for the different simulations. It was just below 8 m for the complete area, and varied slightly for the different sub-areas that were investigated. The smallest mean values were estimated for sub-area Q3, where the time-independent part varied from 6.3–6.6 m. For the other three sub-areas, the spatial fields were quite comparable with estimated mean values close to 8 m. It is obviously not a problem that the average sea state conditions are slightly different for neighbouring geographical areas, but differences in the order of 1.5 m might be surprising. Nevertheless, the mean values for the complete area lie between the values for the various sub-areas, and in this sense, the results are internally consistent. The spatial fields for the smaller sub-areas displayed slightly less spatial variability than for the overall area, but this could be expected since the geographical extent is smaller.

Also the estimated space-time interaction contribution, $\theta(x, t)$, is higher when applied to the whole area compared to either of the sub-areas with higher spatial resolution. For the whole area, the contribution from this component is a variability of 3.55 m, whereas the net contribution for the four sub-areas varies from 1.8 m (Q1) to 2.8 m (Q3). The explanation for this difference is not obvious, but since this component describes a short-term interaction between space and time, it should not be unexpected that the contribution from this component is sensitive to the spatial resolution in the data. It is noted that for the C-ERA-40 data, this component was also found to be sensitive to the temporal resolution (Vanem et al. 2012a).

It is reassuring then to observe that the seasonal component behaves very similarly for all areas that have been investigated. The estimated expected seasonal variation is found to be 5.5 m for three of the sub-areas as well as the overall area. For the last sub-area, Q3, a slightly smaller seasonal variation of 5.3 m is estimated, which is still comparable. Hence, the results for the various sub-sets of the data are deemed to be consistent.

Perhaps the most interesting contribution is the long-term trend that can possibly be partly related to climate change. The estimated trend for the overall area is positive, but not significantly so at the 90 % level. For the three first sub-areas investigated (Q1–Q3), the estimated mean long-term trends are still positive but smaller than the overall trend and still not significantly positive. However, for sub-area Q4, the estimated long-term trend is found to be statistically significant and also slightly stronger than the trend estimated for the area overall. Notwithstanding the different estimates for the trend, the fact that the overall area has an estimated trend that falls between the other estimates suggests that the results are internally consistent. Moreover, the results indicate that there are large uncertainties as to whether there are any significant trends, but that the north-easterly corner of the overall area are expected to experience a stronger trend than the other parts of the area. The observation that trends are stronger in Q4 agrees well with a previous analysis on the spatial distribution of trends in the wave climate[1].

The trends extracted by the Bayesian hierarchical space-time model are also consistent with the trend estimated by fitting a straight line by least squares. Estimated trends vary from 4 to 35 cm for the different sub-areas, with an estimated trend of 21 cm for the overall area, and this is believed to be consistent with the fitted straight line with an increase of about 29 cm for the spatial mean. Furthermore, the fact

[1] Ole Johan Aarnes (2011), *Trends in Wave Height and its Relation to Cyclone Activity in the NE Atlantic*. Presented at the 12th International Workshop on Wave Hindcasting and Forecasting & 3rd Coastal Hazard Symposium and available online at http://www.waveworkshop.org/12thWaves/Presentations/B1.pdf

that most of the estimated trends are not statistically significant at the 90 % level agrees with the results for the least square fitted linear trend (see Table 4).

The future projections are a result of the estimated long-term trends in the data. Hence, it is expected that future projections for sub-area Q4 are higher than for the other areas. This is indeed what is observed, but the uncertainties are large and the future projections for all areas fail to be statistically significant. Estimated mean future projections towards the year 2100 range from 27 cm (sub-area Q1) to 2.3 m (sub-area Q4) with an estimated expected increase of 1.9 m for the area overall, assuming emission scenario A2. For scenario B1, the corresponding range of mean estimates is from 9 to 72 cm. These results are regarded as internally consistent, even though no statistically significant future projection of monthly maximum significant wave height is found.

Some control runs for three of the investigated areas were performed in order to see if increasing the burn-in would influence the results, i.e. for the overall area and for sub-areas Q3 and Q4. These control runs indicate that results for all but one of the model components are robust to changes in burn-in length, but that the spatial field estimates are somewhat sensitive to increased burn-in period. The spatial patterns of the estimated fields are similar but the estimated average levels are different for the initial and control runs. This is troublesome and indicates that the time-independent component might fail to converge within the burn in period. Hence, the results for this particular component are less trustworthy. This also raises the question of whether the other components area affected and to what extent. Obviously, all components in the model are interconnected, but it appears from the results that the other components are not very sensitive to the length of the burn in period. This indicates that possible convergence problems are isolated to the spatial field component, even though this cannot be assured. It is also unexpected that only the average level of the spatial field is affected and that the model is able to consistently describe the spatial patterns of the fields.

One explanation for the possible lack of convergence is that the spatial field is quite large (many data points), and that it therefore takes time to explore the complete state space for the parameters obtained by the Metropolis-Hastings steps. These were drawn from a proposal distribution, and if the spatial field is large, the joint distribution might be very narrow leading to only small steps. However, the acceptance rate for the Metropolis-Hastings step is quite high in the simulations. Another explanation could be that the model is over-parametrised in the spatial component so that there are many solutions that lead to a reasonable fit. Possibly, the joint posterior distribution might be multimodal, making it difficult to estimate the posterior mean reliably by MCMC.

At any rate, it is observed that the results for all components except for the estimated average level of the spatial field are consistent and that the extended burn in period does not significantly alter these estimates. In particular, the results agree on an increasing, albeit not statistically significant, trend for all areas except the sub-area Q4 where the estimated trend is significantly increasing also for the control run. It is reassuring to observe that this particular result is in agreement with previous studies.

5.2 Comparison with previous results obtained with C-ERA-40 data

As has been stressed above, direct comparison of results from the analyses of the NORA10 data and the C-ERA-40 data is not valid due to several reasons. Nevertheless, it is deemed interesting to discuss some of the similarities and differences between the two analysis outcomes and a crude comparison of the results will be presented in this subsection.

Comparing the estimated spatial fields, it is observed that it is less spatial variation in the NORA10 data than what was observed in the C-ERA-40 data. Since the NORA10 data covers a significantly smaller geographical area, this is reasonable. It is also observed that the range of contributions for the space-time dynamic part is of comparable order of magnitude, but with a slightly larger contribution from this term for the NORA10 data. This could possibly be explained by the higher spatial resolution of the NORA10 data, which might describe more of the short-term dynamics of the sea states. The estimated seasonal contributions are comparable, with perhaps slightly larger seasonal variation in the NORA10 data compared to the C-ERA-40 data.

The NORA10 data display less significant long-term trends compared to the results for the C-ERA-40 data. In fact, the identified trends in the NORA10 data are only statistically significant for one of the sub-areas that are investigated, i.e. Q4, whereas the models pick up a statistically significant increasing trend in the C-ERA-40 data. This result is confirmed by the spatiotemporal model and was also found by fitting a straight line by least squares.

One obvious explanation for the different results could be the difference in the geographical areas; although the areas are largely overlapping, they are not identical. Furthermore, trends are known to be varying spatially in a way that is not captured by the model (which assumes a spatially homogeneous trend over the area). Hence, the different geographical coverage of the C-ERA-40 and the NORA10 data subject to analysis may explain, at least partly, the differences in estimated long-term trends.

Another explanation for these discrepancies might be the difference in the temporal span. The C-ERA-40 data previously investigated only covered the period until 2002, whereas the NORA10 data covers the period until 2012. A very crude investigation into the NORA10 data suggests that there is an increasing trend from 1958 until 2002 followed by a very slight decreasing trend from 2002 until 2012, for the spatial mean and spatial max time series. However, none of these trends are statistically significant. Furthermore, for the spatial min time series, the trend in the data is increasing throughout the period, although never being statistically significant.

It is also noted that the NORA10 data were obtained by downscaling of ERA-40 data and running a WAM model forced by ERA-40 wind fields. When a similar analysis was performed on ERA-40 wind speeds, no particular long-term trends were picked up in the wind-speed data (Vanem and Breivik 2013). Hence, one possible explanation could be that NORA10 does not pick up the trends in the ERA-40 data of significant wave height since these are not reflected in the wind speed data. It should be emphasized that the ERA-40 data for significant wave height have not been investigated, only the corrected C-ERA-40 data. Possibly, the trends in the C-ERA-40 data may not be present in the original ERA-40 data and may have been introduced by the correction measures applied to ERA-40 to obtain C-ERA-40

6 Summary and conclusions

The Bayesian hierarchical space-time models for significant wave height that have previously been applied to C-ERA-40 data have been applied to NORA10 data for an overlapping area in the North-East Atlantic in this paper. Overall, the model seems to perform well in describing the temporal and spatial variations in the data, although the estimates pertaining to the average time-independent component are found to be sensitive to the length of the burn-in period.

Based on the analysis presented herein, it is concluded that there are no significant long-term trends in the overall NORA10 data of significant wave height, although the expected trends are slightly increasing. The results also confirm that trends are location specific, and a statistically significant increasing trend was identified for the north-eastern quarter of the area. Furthermore, due to the absence of any clear trend, future projections obtained by extrapolation beyond the support of the data are highly uncertain and should be used with care. Thus, whether there are any actual trends in the overall North-Atlantic wave climate and whether there will be any future increases in the wave climate in the current century remains highly uncertain and inconclusive. More studies are hence needed in order to provide a better understanding and knowledge about trends in the wave climate, including quantification of the uncertainties involved.

Interestingly, the results from this analysis pertaining to long-term trends seem to contradict previous results derived from C-ERA-40 data of significant wave height. Whereas the analysis of the C-ERA-40 data suggested that there are statistically significant increasing long-term trends over the area, the identified trends in the NORA10 data are not statistically significant (except for Q4). However, there are many differences between the two data sets, such as geographical coverage, spatial and temporal resolution, time period and correction techniques applied to the data. Therefore, there is no reason to believe that the results from the different studies are not consistent. In particular, acknowledging that trends are highly region specific, the fact that the two studies cover different geographical areas indeed suggest that different trends would be expected.

Future projections made by the model are uncertain and even though an expected future increase in the monthly maximum significant wave height towards the end of the century is estimated, the projections are uncertain with 90 % credible intervals ranging from negative to positive trends.

Acknowledgments The work presented in this paper has been carried out with support from the Norwegian Research Council (RCN) funded project ExWaCli.

Thanks to Ole Johan Aarnes at the Norwegian Meteorological Institute, Bergen for kindly providing the NORA10 data used in the analysis. He also prepared Figure 1. Thanks also to Profs. Bent Natvig and Arne Bang Huseby at University of Oslo for valuable discussions and to Dr. Elzbieta Bitner-Gregersen at DNV-GL Strategic Research & Innovation for valuable discussions and support.

References

Aarnes OJ, Breivik Ø, Reistad M (2012) Wave extremes in the northeast atlantic. J Climate 25:1529–1543

Bitner-Gregersen EM, Eide LI, Hørte T, Skjong R (2012) Ship and Offshore Structure Design in Climate Change perspective. SpringerBrief in Climate Studies, Springer

Breivik Ø, Aarnes OJ, Bidlot J-R, Carrasco A, Sætra Ø (2013) Wave extremes in the North East Atlantic from ensemble forecasts. J Climate 26:7525–7540

Caires S, Sterl A (2005) A new nonparametric method to correct model data: application to significant wave height from ERA-40 re-analysis. J Atmos Ocean Technol 22:443–459

Caires S, Sterl A, Bidlot J-R, Graham N, Swail V (2004) Intercomparison of different wind-wave reanalyses. J. Climate 17:1893–1913

Caires S, Swail V (2004) Global wave climate trend and variability analysis. Preprints of 8th International Workshop on Wave Hindcasting and Forecasting

Cavaleri L, Bertotti L (2003) The characteristics of wind and wave fields modelled with different resolutions. Q J R Meteorol Soc 129:1647–1662

DNV (2010) Climate change and effect on marine structure design. Tech. rep., Det Norske Veritas. R&I Position Paper 1

DNV (2011) Potential impact of climate change on tanker design. Tech. rep., Det Norske Veritas. R&I Position Paper 8

Furevik R, Birgitte, Haakenstad H (2012) Near-surface marine wind profiles from rawinsonde and NORA10 hindcast. J Geophys Res 117:D23106

IPCC (2001) Climate Change The Scientific Basis. Cambridge University Press

Jain AK, Kheshgi HS, Hoffert MI, Wuebbles DJ (1995) Distribution of radiocarbon as a test of global carbon cycle models. Global Biogeochem Cycles 9:153–166

Komen G, Cavaleri L, Donelan M, Hasselmann K, Hasselmann S, Janssen P (1994) Dynamics and Modelling of Ocean Waves. Cambridge University Press

Moss RH et al. (2010) The next generastion of scenarios for climate change research and assessment. Nature 463:747–756

Reistad M, Breivik Ø, Haakenstad H (2007) A high-resolution hindcast study for the North Sea, the Norwegian Sea and the Barents Sea. Preprints of 10th International Workshop on Wave Hindcasting and Forecasting and Coastal HazardsSymposium

Reistad M, Breivik Ø, Haakenstad H, Aarnes OJ, Furevik BR, Bidlot J-R (2011) A high-resolution hindcast of wind and waves for the North Sea, the Norwegian Sea and the Barents Sea. J Geophys Res 116:C05019

Sterl A, Caires S (2005) Climatology, variability and extrema of ocean waves: the web-based KNMI/ERA-40 wave atlas. Int J Climatol 25:963–977

Swail VR, Cox AT (2000) On the use of NCEP-NCAR reanalysis surface marine wind fields for a long-term North Atlantic wave hindcast. J Atmos Ocean Technol 17:532–545

Thoning KW, Tans PP, Komhyr WD (1989) Atmospheric carbon dioxide at Mauna Loa observatory 2. analysis of the NOAA GMCC data, 1974–1985. J Geophys Res 94:8549–8565

Undèn P et al. (2002) HIRLAM-5 Scientific Documentation. SMHI, Sweden

van Vuuren P, Detlef et al. (2011) The representative concentration pathways: an overview. Clim Chang 109:5–31

Vanem E (2012) Bayesian hierarchical space-time models for significant wave height data. University of Oslo, Ph.D. thesis

Vanem E (2013) Bayesian hierarchical spaec-time models with applications to significant wave height. Springer, Ocean Engineering and Oceanography

Vanem E, Bitner-Gregersen E (2012) Stochastic modelling of long-term trends in the wave climate and its potential impact on ship structural loads. Appl Ocean Res 37:235–248

Vanem E, Breivik ON (2013) Bayesian hierarchical modelling of North Atlantic windiness. Nat Hazards Earth Syst Sci 13:545–557

Vanem E, Huseby AB, Natvig B (2011) 2011: A Bayesian-hierarchical space-time model for significant wave height data. Proc. 30th International Conference on Offshore Mechanics and Arctic Engineering. American Society of Mechanical Engineers (ASME), OMAE

Vanem E, Huseby AB, Natvig B (2012a) A Bayesian hierarchical spatio-temporal model for significant wave height in the North Atlantic. Stoch Env Res Risk A 26:609–632

Vanem E, Huseby AB, Natvig B (2012b) Modeling ocean wave climate with a Bayesian hierarchical space-time model and a log-transform of the data. Ocean Dyn 62:355–375

Vanem E, Huseby AB, Natvig B (2014) Bayesian hierarchical spatio-temporal modelling of trends and future projections in the ocean wave climate with a CO_2 regression component. Environ Ecol Stat 21(2):189–220

Vanem E, Natvig B, Huseby AB (2012c) Modelling the effect of climate change on the wave climate of the world's oceans. Ocean Sci J 47:123–145

Vanem E, Walker S-E (2012) Identifying trends in the ocean wave climate by time series analyses of significant wave height data. Ocean Eng 61:148–160

Wang XL, Swail VR (2002) Trends of Atlantic wave extremes as simulated in a 40-year wave hindcast using kinematically reanalyzed wind fields. J Clim 15:1020–1035